ASTROBIOLOGY
Volume 7, Number 6, 2007

DOI: 10.1089/ast.2007.0150

Research Paper

Radiolytic Hydrogen and Microbial Respiration in Subsurface Sediments

CARLY C. BLAIR, STEVEN D'HONDT, ARTHUR J. SPIVACK, and RICHARD H. KINGSLEY

ABSTRACT

Radiolysis of water may provide a continuous flux of an electron donor (molecular hydrogen) to subsurface microbial communities. We assessed the significance of this process in anoxic marine sediments by comparing calculated radiolytic H_2 production rates to estimates of net (organic-fueled) respiration at several Ocean Drilling Program (ODP) Leg 201 sites. Radiolytic H_2 yield calculations are based on abundances of radioactive elements (uranium, thorium, and potassium), porosity, grain density, and a model of water radiolysis. Net respiration estimates are based on fluxes of dissolved electron acceptors and their products. Comparison of radiolytic H_2 yields and respiration at multiple sites suggests that radiolysis gains importance as an electron donor source as net respiration and organic carbon content decrease. Our results suggest that radiolytic production of H_2 may fuel 10% of the metabolic respiration at the Leg 201 site where organic-fueled respiration is lowest (ODP Site 1231). In sediments with even lower rates of organic-fueled respiration, water radiolysis may be the principal source of electron donors. Marine sedimentary ecosystems may be useful models for non-photosynthetic ecosystems on early Earth and on other planets and moons, such as Mars and Europa. Key Words: Radiolysis—Hydrogen—Subsurface—Biosphere—Sediment—Microbe-mineral interaction—Radiation. Astrobiology 7, 951–970.

INTRODUCTION

Several studies have proposed that deep subsurface microbial communities may rely on molecular hydrogen (H_2) generated abiogenically by water-rock interactions as their primary electron donor (*e.g.*, Pedersen, 1993; Stevens and McKinley, 1995; Chapelle *et al.*, 2002; Lin *et al.*, 2005). Such communities can serve as models for potential ecosystems on other worlds, such as Mars and Europa (*e.g.*, Boston *et al.*, 1992; Fisk and Giovannoni, 1999). Proposed abiotic sources of hydrogen include tectonic activity (Chapelle *et al.*, 2002), serpentinization (Mével, 2003; Kelley *et al.*, 2005), and water radiolysis (Pedersen, 1997). Pedersen (1997) and Lin *et al.* (2005) noted that molecular hydrogen and oxidants produced by the radiolysis of water potentially provide a continuous source of energy to subsurface microbial communities. It is to this hydrogen source that we have directed our focus.

In water-rock systems such as water-saturated

Graduate School of Oceanography, University of Rhode Island, Narragansett, Rhode Island.

sediments, alpha, beta, and gamma radiation released by the decay of radioactive elements dissociates water molecules. Uranium (^{238}U), thorium (^{232}Th), and potassium (^{40}K) are the primary sources of naturally occurring radiation in sediments. Transfer of energy from the alpha, beta, or gamma radiation to water molecules along the radiation track excites and ionizes the water molecules. Short-lived reactive species formed through interactions of the water molecules and found after $\sim 10^{-11}$ s are aqueous electrons (e^-_{aq}), protons (H^+), hydrogen radicals ($H\cdot$), and hydroxyl radicals ($OH\cdot$), the so-called "primary products of water radiolysis" (Draganic and Draganic, 1971). Molecular hydrogen is formed by subsequent reactions on timescales of $\sim 10^{-12}$ to $\sim 10^{-9}$ seconds (Harris and Pimblott, 2002). After $\sim 10^{-9}$ s, the major products of water radiolysis present are: e^-_{aq}, H^+, $H\cdot$, $OH\cdot$, hydrogen peroxide (H_2O_2), and molecular hydrogen (H_2).

Marine sediments, especially those comprised mostly of clay, are a particularly interesting environment for the study of this process. While U, Th, and K concentrations in these sediments are expected to be similar to those in igneous continental crust (Taylor and McLennan, 1985), the grain size of sediments is much smaller, porosity is orders of magnitude higher, and water is distributed throughout the sediment. Therefore, it can be reasonably expected that rates of water radiolysis per volume of bulk material will be much higher in these sediments than in continental crust.

The primary objectives of this study were to determine (1) whether radiolysis of water may be a significant source of biologically accessible energy in anoxic subseafloor sediments [collected during Ocean Drilling Program (ODP) Leg 201] and (2) whether the potential significance of radiolysis in anoxic sediments varies predictably from one subseafloor environment to another (*e.g.*, as a function of lithology, organic flux to the sediment, or rates of microbial activities).

MATERIALS AND METHODS

H_2 production by radiolysis of pore water in deep subseafloor sediments was estimated using U, Th, and K abundances, shipboard measurements of porosity and density, and a model of water radiolysis. To assess geographic variation in the potential rates of radiolytic H_2 production, we compared estimates of radiolytic H_2 yield at equatorial Pacific sites (ODP Sites 1225 and 1226), continental shelf sites (ODP Sites 1228 and 1229), a continental slope site (ODP Site 1230), and an open ocean (Peru Basin) site (ODP Site 1231).

The potential importance of water radiolysis as an energy source was assessed by comparing calculated radiolytic H_2 production rates to estimates of organic-fueled respiration (as net potential carbon oxidation) from D'Hondt *et al.* (2004) at sites with low (Site 1231), intermediate (Sites 1225 and 1226), and high (Site 1230) organic carbon content and microbial activity.

Because grain size affects the extent to which radioactive elements in sediments interact with water, the applicability of this model to deep-sea sediments was assessed by characterizing the grain size distribution at Site 1231.

Site and sample selection

The sites selected for this study were cored during Ocean Drilling Program (ODP) Leg 201 (D'Hondt *et al.*, 2003) (Fig. 1). Sites 1225 and 1226 are located in the eastern equatorial Pacific beneath the relatively high-productivity equatorial ocean at depths of 3760 m and 3297 m, respectively (Shipboard Scientific Party, 2003a, 2003b). Sites 1227, 1228, and 1229 are located on the Peru Shelf beneath the high-productivity Peru upwelling system at water depths of 427 m, 252 m, and 150 m, respectively (Shipboard Scientific Party, 2003c, 2003d, 2003e). Site 1230 is located on the lower continental slope in the accretionary wedge of the Peru Trench at a water depth of 5086 m (Shipboard Scientific Party, 2003f). Site 1231 is located in the Peru Basin at a water depth of 4827 m (Shipboard Scientific Party, 2003g).

Radiolytic hydrogen production rates were calculated for Sites 1225, 1226, 1228, 1229, and 1230 using estimates of ^{238}U, ^{232}Th, and ^{40}K concentrations derived from natural gamma radiation (NGR) spectra (NGR and concentration data from Shipboard Scientific Party, 2003a, 2003b, 2003d, 2003e, 2003f). At these sites, downhole logs of NGR were measured using a Hostile Environment Natural Gamma Ray Sonde (HNGS), which collects 256-channel spectral data; U, Th, and K concentrations are estimated from the HNGS data by proprietary software of Schlumberger (the HNGS manufacturer) (D'Hondt *et al.*, 2003).

Such calculations cannot be made for Sites 1227 and 1231 because downhole logs of NGR were

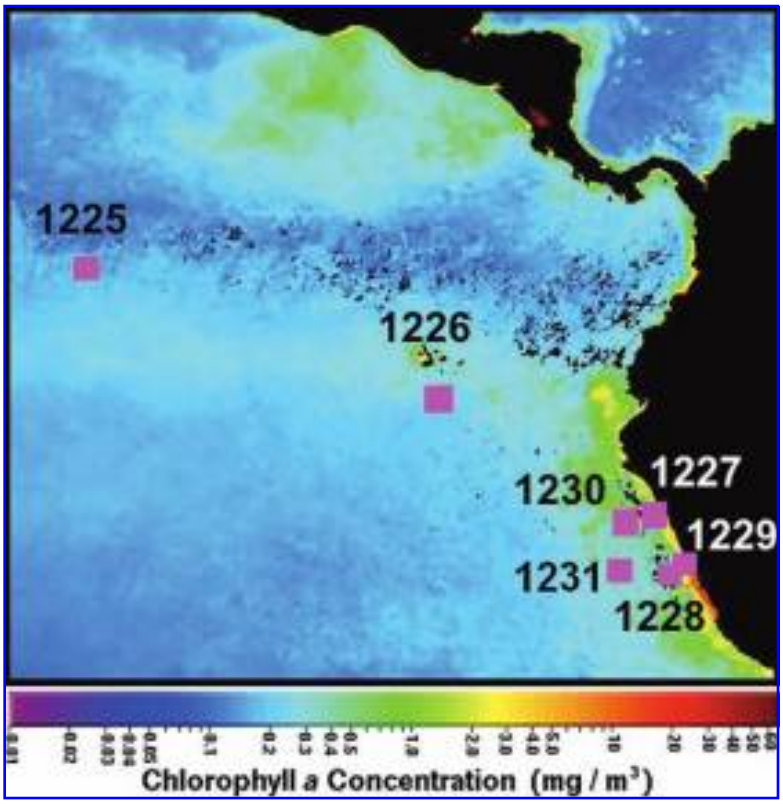

FIG. 1. Map of sea-surface chlorophyll concentrations with Ocean Drilling Program (ODP) Leg 201 site locations (D'Hondt *et al.*, 2003). Subseafloor metabolism fueled by organic carbon varies with chlorophyll content of the surface ocean because organic flux to the sediment depends on the rate of biological production in the surface ocean (D'Hondt *et al.*, 2004). Base map (chlorophyll) edited from a NASA image (http://oceancolor.gsfc.nasa.gov).

not collected at those sites. Although NGR spectral data were measured from the sediment cores of all Leg 201 sites on the ODP multi-sensor track (MST) apparatus (D'Hondt *et al.*, 2003), the MST NGR apparatus was not calibrated appropriately for precisely quantifying U, Th, and K concentrations. For Site 1231, we resolved this issue by making direct measurements of ^{238}U, ^{232}Th, and ^{40}K concentrations using inductively coupled plasma mass spectrometry (ICP-MS). For this purpose, thirty-two 10 cm^3 samples were taken from the archived sediment cores of Hole 1231B. The depths from which the 32 samples were collected range from near the sediment surface to a depth of about 114 meters below seafloor (mbsf). Regions that appeared to be more lithologically variable, based on core photos and core logs of NGR (data from Shipboard Scientific Party, 2003g), were sampled more heavily than those that were apparently more homogeneous.

The number of samples chosen for the Site 1231 analyses was determined by: (1) dividing the sediment column into NGR subunits (based on NGR core logs from Shipboard Scientific Party, 2003g), (2) treating the data within each subunit as a normal population, and (3) using the Standard Normal Distribution Function (Hogg and Ledolter, 1992) to determine the number of samples from each subunit necessary to have a >90% chance that their mean NGR value was within 1 standard deviation of the mean of the population.

Model of water radiolysis

The production of hydrogen by radiolysis of water in a porous medium was calculated using the following equations. The variables and units used are described in Table 1.

Hydrogen production by water radiolysis is due to alpha, beta, and gamma radiation, and can be written as:

$$P_{H_2 sed} = P_{H_2,\alpha} + P_{H_2,\beta} + P_{H_2\gamma} = (G_{H_2,\alpha} D_\alpha) + (G_{H_2,\beta} D_\beta) + (G_{H_2,\gamma} D_\gamma) \quad (1)$$

where $G_{H_2,\alpha}$, $G_{H_2,\beta}$, and $G_{H_2,\gamma}$ are the radiolytic H_2 yields per unit of energy produced in pure water by radiolysis and D_α, D_β, and D_γ are respectively the alpha, beta and gamma radiation doses absorbed by water in the bulk sediment. G_{H_2} values of 1.57×10^4, 5.3×10^3, and 4.5×10^3 H_2 molecules/MeV were used for alpha, beta, and gamma radiation, respectively, and were calculated from Spinks and Woods (1990). [These

Table 1. Variables and Units Used

i.	ρ_r	grain density (g/cm^3_{rock})
ii.	$\overline{A}_x$	activity of nuclide x ($Bq/g_{dry\ sediment}$), where x is ^{238}U, ^{235}U, ^{232}Th, or ^{40}K [a Becquerel (Bq) is a unit of radioactive decay equal to 1 decay/s]
iii.	$\Sigma E_{i,x}$	sum of radiation energy ($i = \alpha$, β, or γ) associated with the decay of nuclide x and its daughters (which are assumed to be in secular equilibrium) (MeV)
iv.	ϕ	porosity (fraction of void space in bulk sediment)
v.	S_i	ratio of radiation stopping power of water to quartz for radiation type i ($i = \alpha$, β, or γ)
vi.	$D_{i,x}$	dose of radiation of type i ($i = \alpha$, β, or γ) absorbed by water in a volume of bulk sediment ($MeV/s/cm^3_{H_2O}$)

values differ from the $G_{H_2,\alpha}$, $G_{H_2,\beta}$, and $G_{H_2,\gamma}$ values of 9.6×10^3, 6×10^3, and 4×10^3 H_2 molecules/MeV, respectively, used by Lin *et al.* (2005), who determined $G_{H_2,\gamma}$ experimentally and appear to have taken $G_{H_2,\beta}$ from Harris and Pimblott (2002).] These values are the greatest source of uncertainty in our calculations because they were not measured at *in situ* conditions. However, they are affected very little by changes in temperature and pressure, and they change very little over a wide range of pH (Draganic and Draganic, 1971). They are enhanced to some extent by salinity because some inorganic solutes, such as Cl^- and CO_3^{2-}, react with OH· and thereby impede the H_2-limiting reaction where OH· combines with H_2 to form H_2O and H· (Spinks and Woods, 1990; Lin *et al.*, 2005). For example, Lin *et al.* (2005) reported ~20% higher H_2 yields in anaerobic water at pH 7 with 0.5 *M* NaCl than in pure anaerobic water at pH 7. However, H_2 is generally unreactive once it is formed because of its low solubility in water and its high bond dissociation energy (Spinks and Woods, 1990).

The radiation dose for a given type of radiation is due to contributions from the decay series of ^{238}U, ^{235}U, ^{232}Th, and ^{40}K:

$$D_\alpha = D_{\alpha,^{238}U} + D_{\alpha,^{235}U} + D_{\alpha,^{232}Th} \quad (2a)$$

$$D_\beta = D_{\beta,^{238}U} + D_{\beta,^{235}U} + D_{\beta,^{232}Th} + D_{\beta^{40}K} \quad (2b)$$

$$D_\gamma = D_{\gamma,^{238}U} + D_{\gamma,^{235}U} + D_{\gamma,^{232}Th} + D_{\gamma,^{40}K} \quad (2c)$$

Note that the alpha radiation dose does not include a contribution from ^{40}K because this isotope does not undergo alpha decay. Using Equations 2a–2c, Equation 1 can be rewritten as:

$$P_{H_2,sed} = [G_{H_2,\alpha}(D_{\alpha,^{238}U} + D_{\alpha,^{235}U} + D_{\alpha,^{232}Th})] + [G_{H_2,\beta}(D_{\beta,^{238}U} + D_{\beta,^{235}U} + D_{\beta,^{232}Th} + D_{\beta,^{40}K})] + [G_{H_2,\gamma}(D_{\gamma,^{238}U} + D_{\gamma,^{235}U} + D_{\gamma,^{232}Th} + D_{\gamma,^{40}K} \quad (3)$$

The radiation doses can be expressed using measurable quantities:

$$D_{i,^{238}U} = \frac{\rho_r \overline{A}_{^{238}U} \Sigma E_{i,^{238}U}}{\frac{1}{1-\phi} + \frac{1}{S_i \phi}} \quad (4a)$$

$$D_{i,^{235}U} = \frac{\rho_r \overline{A}_{^{235}U} \Sigma E_{i,^{238}U}}{\frac{1}{1-\phi} + \frac{1}{S_i \phi}} \quad (4b)$$

$$D_{i,^{232}U} = \frac{\rho_r \overline{A}_{^{232}U} \Sigma E_{i,^{232}U}}{\frac{1}{1-\phi} + \frac{1}{S_i \phi}} \quad (4c)$$

$$D_{i,^{40}U} = \frac{\rho_r \overline{A}_{^{40}U} \Sigma E_{i,^{40}U}}{\frac{1}{1-\phi} + \frac{1}{S_i \phi}} \quad (4d)$$

where i is alpha, beta, or gamma radiation, ρ_r is grain density (average density of dry sediment grains), $\overline{A}_{^{238}U}$, $\overline{A}_{^{235}U}$, $\overline{A}_{^{232}Th}$, and $\overline{A}_{^{40}K}$ are the activities of ^{238}U, ^{235}U, ^{232}Th, and ^{40}K, respectively, ΣE_i is the energy sum of the decay series of the parent nuclide specified, ϕ is porosity (the fraction of the bulk volume taken up by water), and S_i is the relative stopping power ratio.

Secular equilibrium is assumed for our calculations because the half-lives of the daughters of ^{238}U, ^{235}U, ^{232}Th, and ^{40}K are short compared to the age of all but the shallowest sediments at the Leg 201 sites. Note that the radiation dose reaches a maximum when porosity is 50% and goes to zero as porosity approaches either 0 or 100%. To convert the dose absorbed by the bulk sediment to the dose absorbed by water, multiply equations 4a–4d by $1/\phi$. Grain density and porosity data are from D'Hondt *et al.* (2003). Activities were calculated using ^{238}U, ^{232}Th, and ^{40}K concentrations determined by ICP-MS or derived from downhole logs of NGR (data from D'Hondt *et al.*, 2003). Uranium-235 concentrations were calculated from ^{238}U concentrations using a constant isotopic abundance value of 0.725%. Decay

series energy sums were calculated using the World Wide Web Table of Radioactive Isotopes (Ekström and Firestone, 1999). S_i values of 1.5, 1.25, and 1.14 were used for alpha, beta, and gamma radiation, respectively, and were taken from Aitken (1985).

ICP-MS analyses of Site 1231 samples

Sediment samples were taken from the working half of Site 1231 cores using plastic mini-corers and stored in sealed plastic bags. The samples were digested for analysis by using a modification of the procedure used by Balzer (1999) and Kelley *et al.* (2003). Subsamples of the sediments were rinsed with deionized water, homogenized, and dried in an oven prior to digestion. Approximately 50 mg of sample were digested for each Site 1231 sample, each calibration standard reference material (SRM), and the quality assurance / quality control (QA/QC) SRM. The Site 1231 samples and the SRMs were digested in parallel. Each sample was digested by adding a 3:1 mixture of 8N HNO_3 and concentrated HF to the sample, heating the mixture on a hot plate at 120°C, and then drying it down. A small amount of water and 3 mL of hydrogen peroxide were subsequently added to each sample to eliminate organic carbon. The samples were re-dissolved with a mixture of 3 mL 8N HNO_3 and 3 mL deionized water, transferred to high-density polyethylene bottles, and then brought to their final dilution factor (~1000X) via the addition of deionized water. The bottles and their contents were sonicated to dissolve any remaining precipitates prior to ICP-MS analysis. A small, known mass of an internal standard (a "spike") that contained 0.393 ppm bismuth (Bi) and 79.72 ppm indium (In) in 2% HNO_3 was added to a split of each sample to achieve concentrations of ~10 ppb Bi and ~2 ppm In.

The spiked solutions were analyzed for ^{238}U, ^{232}Th, and ^{39}K content using a Finnigan MAT ELEMENT High Resolution ICP-MS. All 3 isotopes were measured simultaneously on the single sample dilutions. ^{39}K and ^{40}K concentrations were interconverted using an isotopic abundance value for ^{40}K of 1.17×10^{-4}. Uranium-238 and ^{232}Th were measured using the low-resolution mode of the ELEMENT (~300 M/ΔM), while ^{39}K was measured using the high-resolution mode (~8000 M/ΔM) in order to separate the ^{39}K signal from the nearby ^{40}Ar signal and from the significant polyatomic interferences of $^{38}Ar^{1}H$ and $^{23}Na^{16}O$. Each analytical run consisted of 2 blanks, an external drift correcting solution, 5 calibration SRMs, the QA/QC SRM, and several unknowns. To obtain the ^{238}U, ^{232}Th, and ^{39}K concentrations, raw ICP-MS data were blank-subtracted, corrected for drift, calibrated using the 5 SRMs, and corrected for dilution.

The acid blank contained 2% HNO_3 and was prepared using the same nitric acid and water used during sediment digestion. It was not spiked with the internal standard. The procedural blank contained 2% HNO_3 and resulted from treating an empty beaker identically to the beakers that contained the SRMs and the Site 1231 samples (*i.e.*, the blank was "digested," dried down, redissolved, and spiked with internal standard).

The long-term decrease in instrument sensitivity during a run was corrected for by normalizing the analyte intensities to the change in intensities of the internal standards of Bi (for low-resolution mode) and In (for high-resolution mode).

The external drift corrector was a solution that contained several Site 1231 samples mixed together to achieve matrix matching. It was analyzed after every third sample to correct for changes in instrument sensitivity for each analyte (see, *e.g.,* Cheatham *et al.,* 1993).

The calibration standard reference materials used in this study were volcanic rock standards with certified concentrations of total U, total Th, and total K (Table 2). Based on the NGR-derived concentration estimates at other Leg 201 sites, we anticipated for Site 1231 ^{238}U concentrations in the range of 0.05 ppm to 15 ppm, ^{232}Th concentrations in the range of 1 ppm to 15 ppm, and ^{39}K concentrations in the range of 0.05% to 3%. The SRMs were chosen based on their U, Th, and K concentrations (which for the most part bracketed the anticipated ranges) and their compatibility with the digestion procedure.

The QA/QC SRM was IAEA-315, a marine sediment with certified concentrations of U, Th, and K similar to those predicted for the unknowns. It was used as a check on the accuracy of the analytical methods and was digested and analyzed as an unknown several times throughout the course of the measurements.

Grain size analysis

Grain size analysis was performed on subsamples of each Site 1231 sample. The sample prepa-

Table 2. Summary of Certified Total Thorium (Th), Total Uranium (U), and Total Potassium (K) Concentrations in the Calibration Standard Reference Materials (SRMS) Used in this Study

SRM	*[Th] (ppm)*	*[U] (ppm)*	*[K] (wt %)*
USGS BIR-1	0.031	0.0085	0.025
USGS W-2a	2.1	0.49	0.519
USGS AGV-2	6.1	1.88	2.39
USGS RGM-1	15	5.8	3.57
USGS STM-1	31	9.1	3.55

ration methods used here were adapted from Steurer and Underwood (2003). Samples were weighed to ensure that laser obscuration values (laser obscuration is the percentage of light that is attenuated because of scattering or absorption by the particles, or both) would be high enough for particles to be detected but not so high that particle interaction or overlap would become significant (10–20%). They were then dispersed with sodium hexametaphosphate and treated with hydrogen peroxide for approximately 24 hours to digest organic matter. Clay-rich samples were further dispersed by sonicating for approximately 15 minutes; to avoid disintegration of fragile components (*e.g.*, foraminiferal tests), this step was not used for nannofossil-rich samples. The resulting suspensions were diluted with deionized water and vigorously agitated within the sample dispersion unit.

The diluted suspension aliquots were scanned with a Malvern Mastersizer 2000 laser diffraction-based particle size analyzer. The Fraunhofer model of light scattering was used for all measurements. Mean grain size, standard deviation, skewness, and kurtosis were measured using the Mastersizer 2000 (version 5.22) software.

RESULTS

Relation of calculated radiolytic hydrogen yields to radioactivity and physical properties

We use the Site 1231 data to illustrate relationships between radioactivity, physical properties, and our estimates of radiolytic H_2 yields. Distributions of ^{238}U, ^{232}Th, and ^{40}K with depth are similar to the distribution of natural gamma radiation (NGR), because NGR is almost entirely due to the abundance of these isotopes (Figs. 2A–B). Thus, like NGR, ^{238}U, ^{232}Th, and ^{40}K concentrations are generally higher in the upper portion of the sediment column (0–55 mbsf) but decrease dramatically at the Unit II/III boundary. Average ^{40}K, ^{238}U, ^{235}U, and ^{232}Th concentrations are 2.7 ± 0.0 ppm, 4.2 ± 0.1 ppm, 30.3 ± 0.9 ppb, and 14.8 ± 0.8 ppm, respectively, in the upper half of the sediment column and 0.4 ± 0.0 ppm, 0.5 ± 0.0 ppm, 3.7 ± 0.1 ppb, and 1.0 ± 0.1 ppm, respectively, in the lower half of the sediment column. Note that, because ^{235}U concentrations are much smaller than those of ^{238}U, there is little difference between ^{238}U content and total uranium content; we will hereafter use "U" to refer to total uranium unless an isotope is specified.

Variations in activities of ^{40}K, ^{238}U, ^{235}U, and ^{232}Th with depth follow similar patterns to those of ^{40}K, ^{238}U, ^{235}U, and ^{232}Th concentrations; however, the relative magnitude of activity is different for each element, because each has a different decay constant (Figs. 2B–C). In any given sample, ^{40}K activity is greatest because its concentrations are relatively high and its decay constant is very high. Uranium-238 and ^{232}Th activities are generally of the same order of magnitude and similar because, though ^{232}Th is usually ~3–4 times more abundant, the decay constant of ^{238}U is ~3 times greater. Uranium-235 exhibits relatively high activity, despite its low concentrations, because it has the largest decay constant of these isotopes (approximately twice that of ^{40}K).

Our estimates of H_2 yield with depth exhibit similar patterns as the U, Th, and K concentrations but are modulated by the effect of porosity (Figs. 2B, 2D–E). According to our model, radiation doses reach a maximum when porosity is 50% and go to zero as porosity approaches either 0 or 100%. Because porosity is much closer to 50% in the lower portion of the sediment column, the calculated H_2 yields in this interval are enhanced relative to those in the higher porosity, clay-rich portions of the sediment column. For example, average ^{40}K, ^{238}U, and ^{232}Th concentrations are respectively ~7, ~8, and ~15 times greater in the

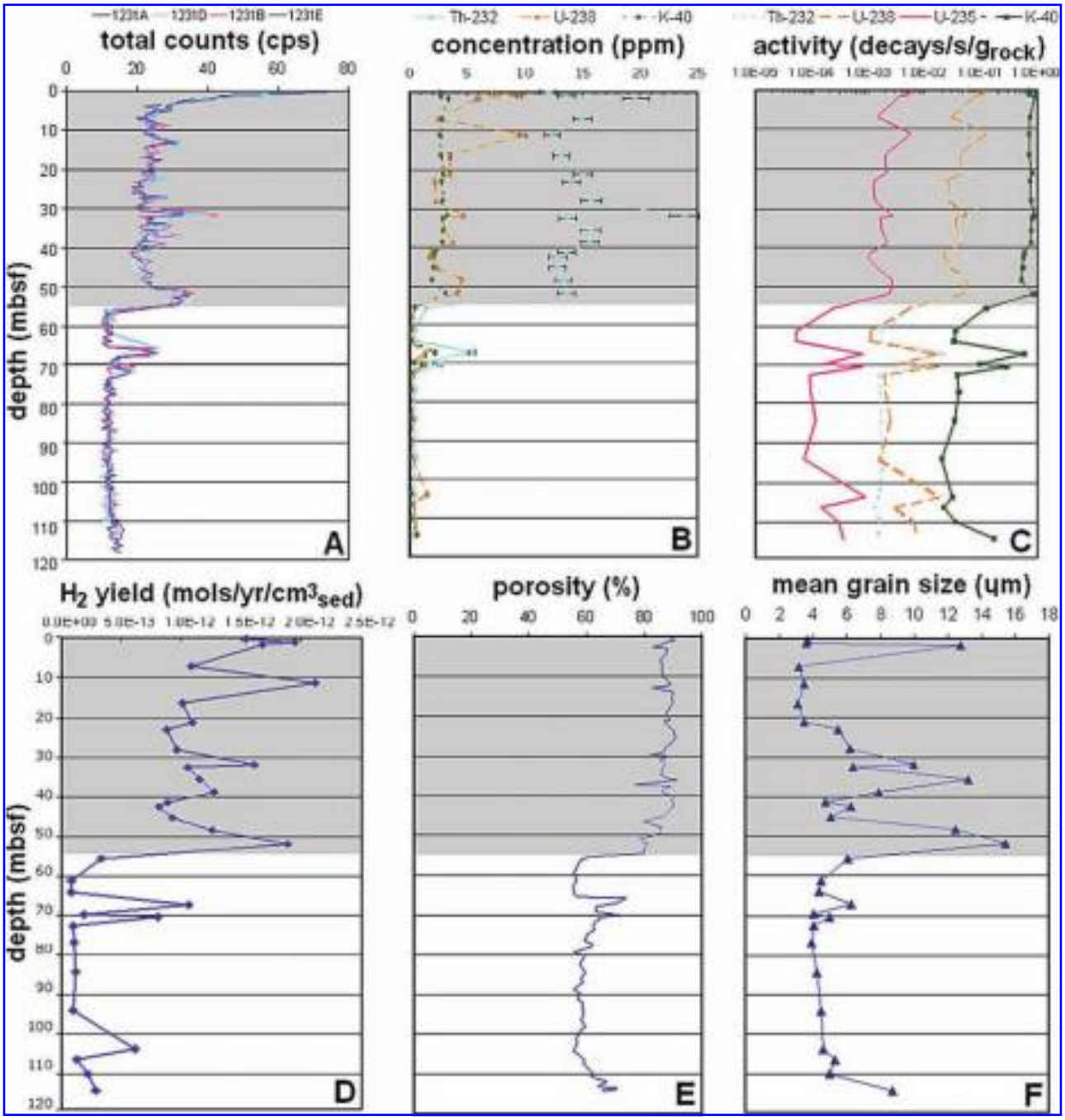

FIG. 2. Depth profiles of physical properties and calculated yields of H_2 from water radiolysis at Leg 201 Site 1231. (**A**) Natural gamma radiation (NGR) profile of cores from 4 holes at Site 1231 (Shipboard Scientific Party, 2003g). The data are plotted as uncorrected average counts per second (cps). (**B**) Concentrations of ^{238}U, ^{232}Th, and ^{40}K, measured using Inductively Coupled Plasma Mass Spectrometry (ICP-MS). (**C**) Activity of ^{238}U, ^{235}U, ^{232}Th, and ^{40}K. (**D**) Calculated radiolytic H_2 production. (**E**) Porosity (Shipboard Scientific Party, 2003g). (**F**) Mean grain size (in μm). The shaded area in the top of each panel marks the depth zone of high gamma ray counts and high radioactive element concentrations. The unshaded area in the bottom of each panel marks the depth zone of low gamma counts and low radioactive element concentrations.

upper portion of the sediment column than in the lower portion, but the average H_2 yield is only ~4 times greater in the upper part of the column. The calculated average radiolytic H_2 yield for the upper half of the sediment column is 1.3×10^{-12} moles $H_2/yr/cm^3_{sed}$, while that of the lower half of the sediment column is 3.0×10^{-13} moles $H_2/yr/cm^3_{sed}$.

Our estimates of H_2 yield with depth differ from the pattern of NGR by not exhibiting a strong peak near the top of the sediment column. This is probably because we did not include a contribution from excess ^{230}Th in our calculations of radiolytic H_2 yield. Although we do not have ^{230}Th concentration data for Site 1231, we can roughly estimate excess ^{230}Th concentrations in the upper part of the sediment column (and, therefore, radiolytic H_2 production due to excess ^{230}Th in the column), by using a calculated ^{230}Th deposition rate. This calculation is based on the principle that, because ^{230}Th is produced at a constant rate by the decay of ^{238}U and has a short residence time in the ocean water column, the flux of ^{230}Th to the seafloor is mainly a function of the depth of the overlying water column (Bacon, 1984). According to this calculation, radiolysis of water by the decay of excess ^{230}Th may produce an additional 1.2×10^{-12} moles $H_2/yr/cm^3_{sed}$ in the top 3 or so meters of sediment at Site 1231, which would nearly double the radiolytic H_2 yield in the uppermost portion of the sediment column. However, because the interval over which this process is significant is such a small fraction of the total height of the sediment column, the decay of excess ^{230}Th does not significantly contribute to total radiolytic H_2 production at this site.

Energy from alpha decay is by far the most important contributor to our calculations of radiolytic H_2 production. It accounts for 88% of the calculated H_2 production, while beta decay energy and gamma radiation account for 10% and 2% of the calculated H_2 production, respectively (Fig. 3A). These proportions are very similar in both the upper and lower halves of the sediment column. Alpha decay is relatively important because alpha radiation is much more energetic and effective at dissociating water molecules than either beta radiation or gamma radiation.

Energy from the decay of ^{238}U series isotopes is the most important contributor to our estimates of radiolytic H_2 production. It accounts for 49% of the calculated H_2 production by radiolysis, while the decay of ^{232}Th, ^{40}K, and ^{235}U series isotopes account for 41%, 8%, and 2% of the calculated radiolytic H_2, respectively (Fig. 3B). The contributions from the ^{238}U, ^{232}Th, ^{40}K, and ^{235}U series are on average 44%, 48%, ~7%, and ~2%, respectively, in the upper half of the sediment column and 56%, 33%, 9%, and 2%, respectively, in the lower half of the column. This modest difference between the upper and lower portions of the column is likely due to greater importance of terrestrial input in the upper half of the column and marine input in the lower half of the column; thorium concentrations that are high relative to ura-

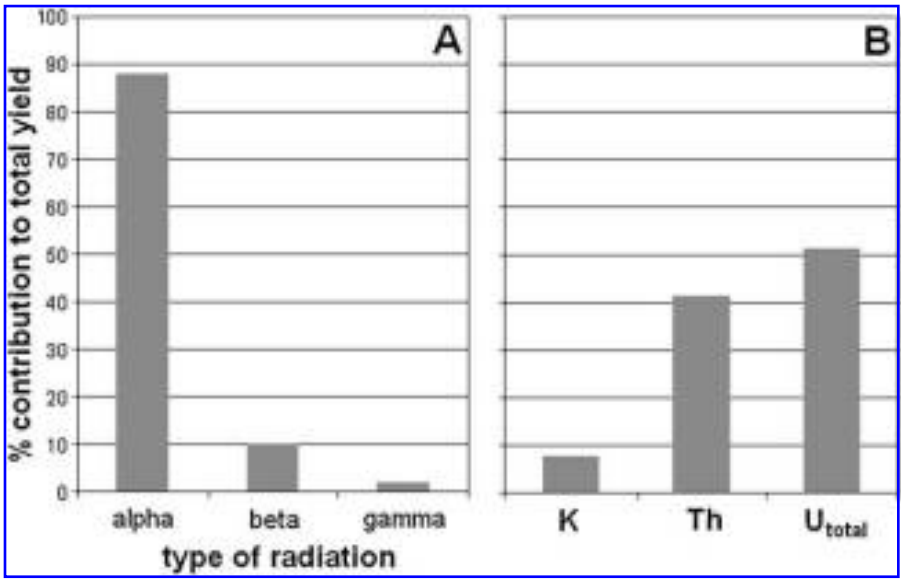

FIG. 3. Contributions to radiolytic H_2 production at Site 1231. (**A**) Relative contribution of alpha decay energy, beta decay energy, and gamma decay energy to calculated radiolytic H_2 yield at Site 1231. Potassium-40 emits beta and gamma radiation, while ^{232}Th, ^{235}U, and ^{238}U emit alpha, beta, and gamma radiation. (**B**) Relative contribution of energy derived from the decay of the potassium (^{40}K), thorium (^{232}Th), and uranium (^{235}U + ^{238}U) series to calculated radiolytic H_2 yield at Site 1231.

nium concentrations are associated with terrestrial input, while uranium concentrations that are high relative to those of thorium are associated with marine input. Calculated H_2 yields due to the decay of ^{238}U and ^{232}Th are much higher than those of ^{40}K despite the higher activity of ^{40}K (Fig. 2C) because ^{238}U and ^{232}Th undergo alpha decay while ^{40}K does not. Although ^{235}U undergoes alpha decay, estimated H_2 yields due to the decay of ^{235}U are low because ^{235}U concentrations are very low. These results imply that a fairly accurate estimate of H_2 production by water radiolysis in fine-grained sediment can be obtained by focusing on the alpha decay of the ^{238}U and ^{232}Th series.

Our model of water radiolysis assumes that sedimentary grains are small enough for radiation from each alpha decay event to escape the grain in which the event originates (diameters <30 μm). However, it is important to note that, once grain size exceeds ~ 30 μm, H_2 yields must decrease because that grain diameter exceeds the stopping distance of alpha radiation (Aitken 1985), and thus, some of the alpha particles will never come into contact with water. At Site 1231, the overall mean grain size is 6.2 μm (Fig. 2F). Mean grain size is 5.0 μm in Unit I, 9.0 μm in Unit II, and 5.0 μm in Unit III. On average, approximately 92% of the sediment grains are in the medium silt and clay size classes (<31 μm). All the samples are mostly medium silt and clay, and 75% of them are over 90% medium silt and clay. We conclude that our assumption is appropriate for estimating H_2 yields from water radiolysis at this site.

Geographic variation in radioactivity and estimated radiolytic H_2 yields

The equatorial Pacific sites (1225 and 1226) had the lowest ^{238}U, ^{232}Th, and ^{40}K concentrations of the Leg 201 sites (Figs. 1, 4A, 5). The Peru Margin sites (1228, 1229, 1230) and the Peru Basin site (1231) have concentrations of ^{238}U, ^{232}Th, and ^{40}K

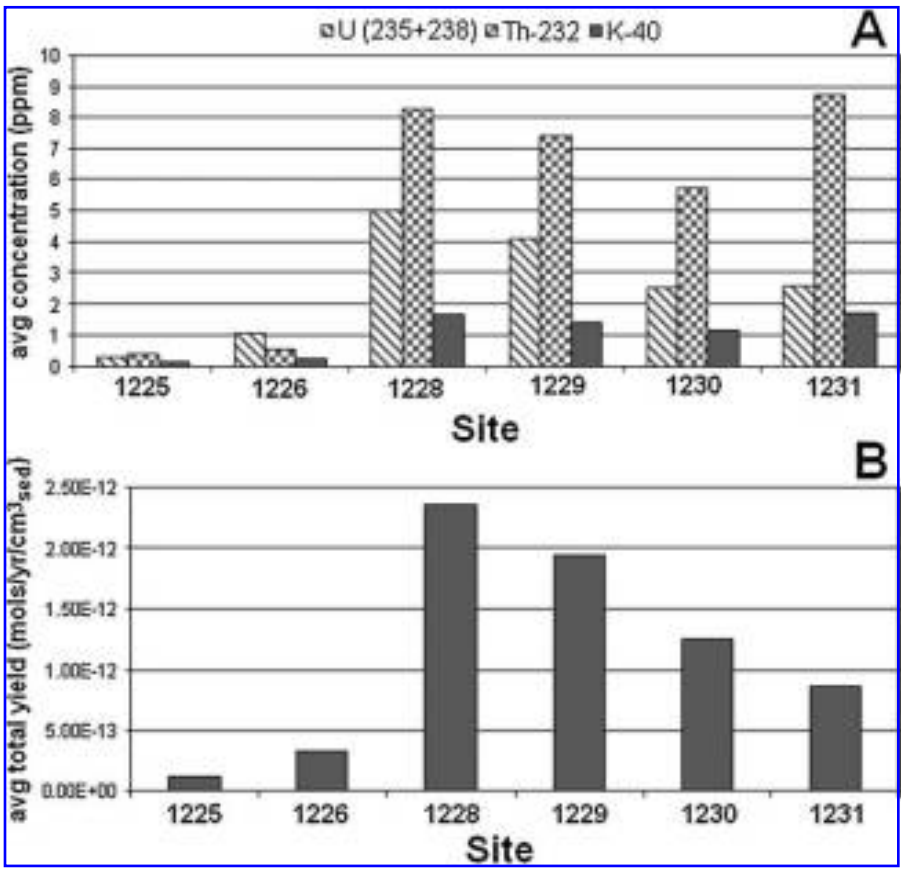

FIG. 4. (A) Average ^{238}U, ^{232}Th, and ^{40}K concentrations at Leg 201 Sites 1225, 1226, 1228, 1229, 1230 [derived from downhole NGR logs, measured using a Schlumberger Hostile Environment Natural Gamma Ray Sonde (D'Hondt *et al.*, 2003)], and Site 1231 (measured using ICP-MS). (**B**) Calculated average radiolytic H_2 yields at the same 6 sites.

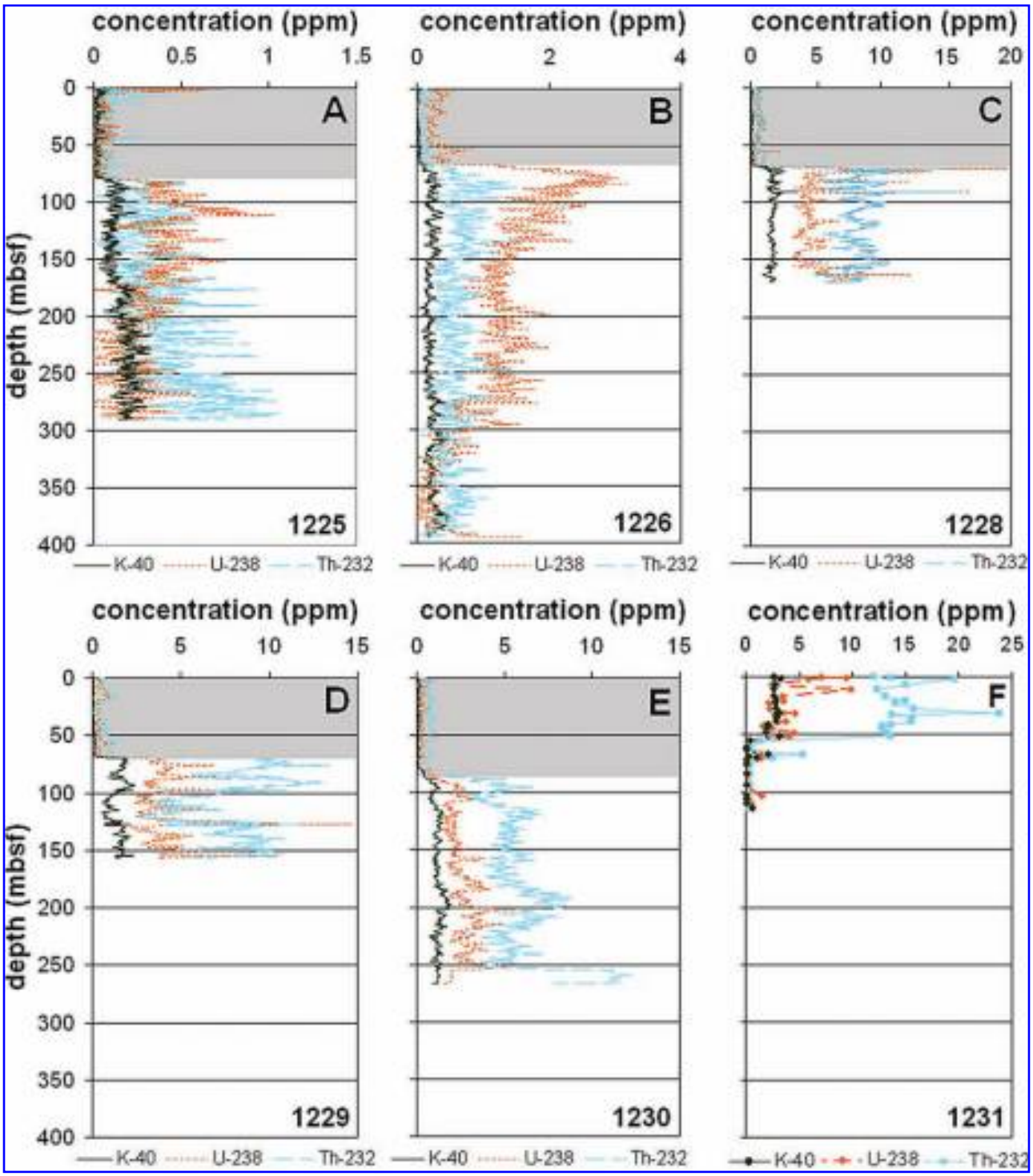

FIG. 5. Concentrations of ^{238}U, ^{232}Th, and ^{40}K as functions of depth at Leg 201 Sites (A) 1225, (B) 1226, (C) 1228, (D) 1229, (E) 1230, and (F) 1231, derived from downhole logs of NGR (A–E) (data from D'Hondt *et al.*, 2003) or measured using ICP-MS (F). The gray area on each plot indicates the interval over which the drill pipe interfered with NGR logging. Note the different depth scale in Panel F.

that are higher and somewhat similar to each other. Our estimates of radiolytic H_2 yields exhibit similar patterns (Figs. 4B, 6). The average calculated yield was lowest at the equatorial Pacific sites (1225 and 1226) and highest at the Peru Margin sites (1230, 1229, and 1228). Although Site 1231 has the highest average concentrations of ^{232}Th and ^{40}K, and fairly high concentrations of

^{238}U, it has a lower average calculated radiolytic H_2 yield than the Peru Margin sites because the latter sites have average ^{238}U concentrations the same as or higher than Site 1231 and much lower average porosities (~65% versus 75% at Site 1231). The calculated average H_2 yields vary by a factor of ~20 between sites.

As at Site 1231, energy from alpha decay is the most important contributor to our calculated radiolytic H_2 production at all these sites. It generates ~90% of the H_2 produced, while beta decay energy and gamma radiation generate ~10% and ~2% of all H_2 production, respectively, with little variation between sites (Fig. 7A). Also, as at Site 1231, energy from the decay of ^{238}U is the most important contributor to our estimates of radiolytic H_2 production at all these sites, followed by energy from the decay of ^{232}Th, ^{40}K, and ^{235}U (Fig. 7B). However, the relative contribution of total U and ^{232}Th to calculated H_2 production varies considerably from site to site. For example, at Site 1226, the decay of total U and ^{232}Th generates 85% and 12% of the calculated H_2 production, respectively, whereas at Site 1230, the decay of total U and ^{232}Th generates 60% and 35% of the H_2 produced, respectively. As with the 2 halves of the sediment column at Site 1231, this difference between sites may be due to differences in the proportions of terrestrial and marine input between sites. These results further support our inference that a fairly accurate estimate of radiolytic H_2 production in fine-grained sediment can be obtained by focusing on the alpha decay of the ^{238}U and ^{232}Th series.

DISCUSSION

Causes of site-to-site variation in calculated radiolytic H_2 production

Lithology controls the rate at which radiolytic H_2 is produced at a given site. In particular, concentrations of radioactive elements, porosity, and grain size are the properties that most strongly influence H_2 production by water radiolysis. Maximum radiolytic H_2 production results when

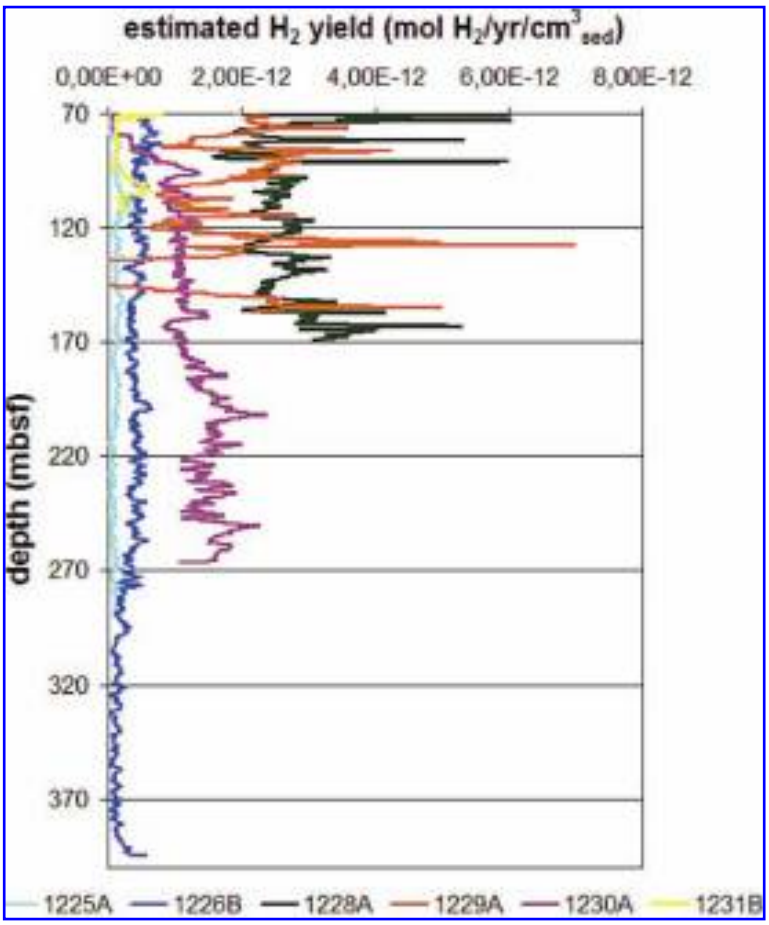

FIG. 6. Calculated radiolytic H_2 yields as functions of depth at five Leg 201 sites. Radiolytic H_2 production rates were calculated using estimates of ^{238}U, ^{232}Th, and ^{40}K concentrations derived from downhole logs of NGR. Calculations were not done for the first 70 meters below seafloor because the drill pipe interfered with measurement of ^{238}U, ^{232}Th, and ^{40}K concentration data over that interval (Fig. 5).

radioactive element concentrations are high, porosity is 50%, and grain sizes are small. These 3 criteria are rarely simultaneously met in marine sediments; for example, terrigenous sediments deposited along continental margins often have relatively high concentrations of radioactive elements and relatively low porosity, but grain sizes often exceed alpha particle stopping distances [as at the Peru Margin ODP sites (Shipboard Scientific Party, 2003c, 2003d, 2003e)]. On the other hand, abiogenic sediments deposited distant from shore (such as at Peru Basin Site 1231) have high concentrations of radioactive elements and small grain sizes but high porosity (Fig. 2). Sediments that are predominantly biogenic (such as those at equatorial Pacific Sites 1225 and 1226) have relatively low porosity and small grain sizes but relatively low concentrations of radioactive elements. The competing effects of these physical properties cause radiolytic H_2 production in the Leg 201 sediments to vary over a range that is surprisingly narrow, given the wide variety of lithologies present (1 order of magnitude).

The potential importance of radiolysis as a source of electron donors to subseafloor communities

The potential importance of water radiolysis as a source of electron donors can be assessed by comparing the calculated radiolytic hydrogen production of each drilled sediment column to previously calculated rates of organic oxidation in the same sediment column. This comparison provides a measure of the potential importance of *in situ* water radiolysis for fueling subseafloor respiration, relative to burial of organic matter from the surface photosynthetic world.

The total radiolytic hydrogen production of each drilled sediment column depends on both the H_2 yield (moles/yr/cm^3) and the depth to which the sediment was drilled (Table 3). It varies by a factor of ~12 between sites. It is low at the

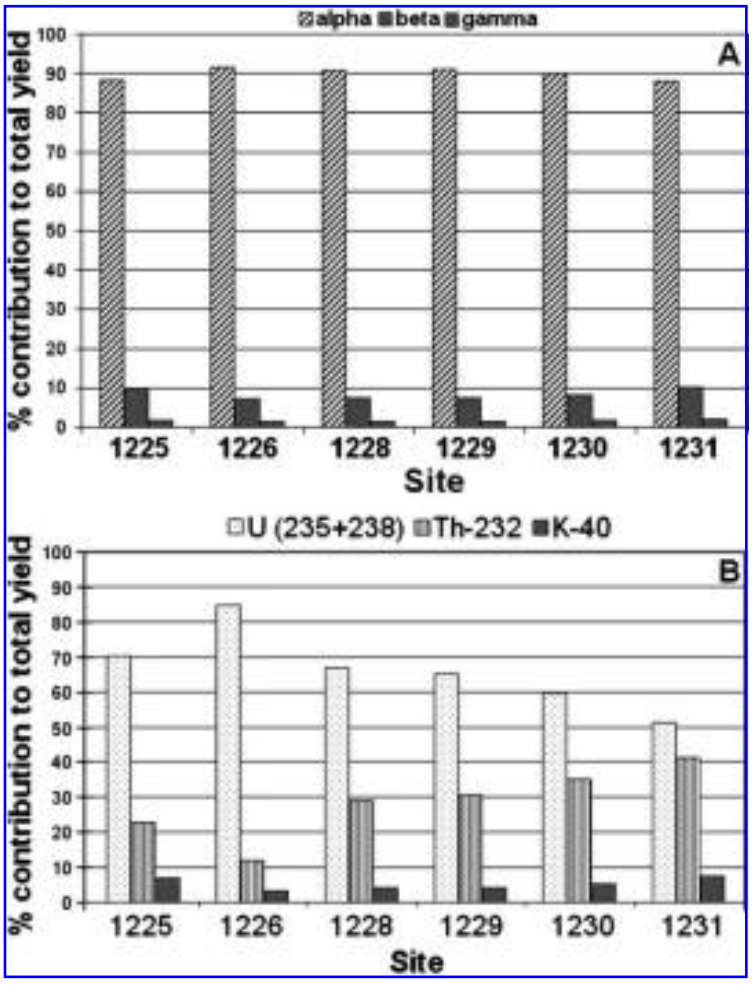

FIG. 7. Contributions to radiolytic H_2 production at six Leg 201 sites. (**A**) Relative contribution of alpha decay energy, beta decay energy, and gamma decay energy to calculated radiolytic H_2 yield at ODP Sites 1225, 1226, 1228, 1229, 1230, and 1231. (**B**) Relative contribution of energy from decay of the potassium (^{40}K), thorium (^{232}Th) series, and uranium (^{235}U + ^{238}U) series to calculated radiolytic H_2 yield at the same sites. Note that energy from the decay of the ^{235}U series consistently contributes 2–3%; its contributions are combined with those of ^{238}U for the sake of graphical simplicity.

Table 3. Site Location, Water Depth, Depth to Which the Sediment Was Drilled, Calculated Radiolytic H_2 Production of the Drilled Sediment Column, Net Respiration [Calculated from D'Hondt *et al.* (2004), Converted to Moles of H_2 Equivalents], and the Ratio of H_2 Production to Respiration (Presented as a Percentage)

Locaiton	*Water depth (mbsl)*	*Depth drilled (mbsf)*	*Radiolytic H_2 production (moles/yr/cm$^2_{sed}$) in drilled sed. column*	*Net respiration (moles H_2 eq/yr/cm$^2_{sed}$)*	*Ratio × 100 (%)*
Ocean margin sites					
Peru Shelf Site 1227	427	151.1	n.d.	3.66E-06	—
Peru Shelf Site 1229	152	194.4	3.77×10^{-8}	n.d.	—
Peru Shelf Site 1228	262	200.9	4.74×10^{-8}	n.d.	—
Peru Slope Site 1230	5086	278.3	3.51×10^{-8}	1.01E-05	0.4
Open ocean sites					
Equat. Pacific Site 1226	3760	420.0	1.31×10^{-8}	6.02E-07	2.2
Equat. Pacific Site 1225	3297	319.6	3.91×10^{-9}	1.14E-07	3.4
Peru Basin Site 1231	4813	121.9	9.79×10^{-9}	1.00E-07	9.8

mbsf, meters below seafloor; mbsl, meters below sea level; n.d., not determinable.

open ocean sites and high at the Peru Margin sites (Table 3).

D'Hondt *et al*. (2004) estimated rates of organic matter oxidation at Leg 201 sites from fluxes of electron acceptors (SO_4^{2-} and NO_3^-) into the sediment column and fluxes of reduced metals (Fe^{2+} and Mn^{2+}) within the sediment column reduction at several Leg 201 sites (Table 3). The sum of these processes at each site is approximately equal to the net rate of electron acceptor reduction at that site. Burial rates of organic matter (D'Hondt *et al.*, 2004) and, for Site 1226, mass balance calculations of dissolved carbon fluxes and rates of carbonate mineral precipitation demonstrate that this net rate of electron acceptor reduction is approximately equal to the gross rate of organic carbon oxidation at each site (Wang *et al.*, 2006). Because water radiolysis generates an electron donor and an electron acceptor in stoichiometric balance (*e.g.*, H_2 and $^1/_2O_2$), metabolic use of radiolytic products does not contribute to net rates of electron acceptor reduction.

The net rate of electron acceptance (net respiration) varies by a factor of ~100 from one Leg 201 site to another (D'Hondt *et al.*, 2004). It is much lower at the open ocean sites than at the ocean margin sites. It is lowest at Peru Basin Site 1231, intermediate at the equatorial Pacific sites (1225 and 1226), and highest at the Peru Margin sites. This geographic variation in net respiration closely resembles the pattern of geographic variation in sea-surface chlorophyll concentration and in the flux of organic matter to the seafloor (D'Hondt *et al.*, 2004). The similarity of these patterns presumably results from the dependence of net respiration on buried organic matter. The flux of organic matter to the seafloor depends, in large part, on the rate of photosynthetic productivity in the overlying ocean (which in turn depends on concentrations of chlorophyll) and on water depth (the distance over which marine organic matter is degraded as it falls to the seafloor) (*e.g.*, Jahnke, 1996). Consequently, net respiration in subseafloor sediments is highest along ocean margins, where photosynthetic productivity is very high and water depth is very low (*e.g.*, at Peru Margin Sites 1227 and 1230). It is lower in the equatorial region where upwelling sustains lower productivity than along the ocean margins and where water depth is much greater (*e.g.*, at the equatorial Pacific Sites 1225 and 1226). It is still lower in open-ocean regions where photosynthetic productivity is lower than in upwelling regions and where water depth is as great or greater than in the upwelling regions (*e.g.*, Peru Basin Site 1231).

Our calculated ratio of radiolytic H_2 production to net respiration (organic oxidation) in each drilled column varies from site to site by a factor of 25 (Table 3). From site to site, this ratio varies inversely with net respiration. It depends more strongly on the rate of net respiration than on the rate of radiolytic H_2 production because net respiration varies by 2 orders of magnitude from site to site, whereas the calculated rate of radiolytic H_2 production varies by only an order of magnitude from site to site. The ratio is lowest at Peru Margin Site 1230 (0.4%), where net respiration of the drilled column is highest, and highest at Site 1231 (9.8%), where net respiration is lowest.

At the open ocean sites (1225, 1226, 1231), these ratios apply to the entire sediment column because those sites were drilled to the basaltic basement. However, this only applies to the upper portion of the sediment column at Peru Margin Site 1230 because only the uppermost portion of the sediment column was drilled at the Peru Margin sites (1227, 1228, 1229, 1230). At these sites, the radiolytic H_2 production of the entire sediment column (drilled and undrilled) is probably much higher than the radiolytic H_2 production of the drilled sediment column that is presented in Table 3.

For two reasons, the ratio of radiolytic H_2 production to net respiration is less well-constrained at Peru Margin site 1230 than at the open ocean sites (1225, 1226, and 1231). First, the radiolytic H_2 yields calculated for the Peru Margin sites may be overestimates because many sediment grains at the Peru Margin sites are larger than the $\sim$30 μm length of an alpha track. Sediment grains at these sites range up to gravel in size (>2000 μm) (Shipboard Scientific Party, 2003c, 2003d, 2003e). Second, net respiration rates calculated by D'Hondt *et al.* (2004) for Peru Margin Sites 1227 and 1230 probably underestimate the net respiration in the entire sediment columns of those sites. A recent radiocarbon study demonstrated that sedimentation rates are very high at these sites (Skilbeck and Fink, 2006); consequently, electron donors such as methane and acetate that are abundant deep in the sediment column may be buried faster than they can diffuse up to be oxidized by SO_4^{2-} reduction in the shallower sediments. To the extent that radiolytic H_2 production is overestimated and net respiration underestimated for Peru Margin sites, radiolytic H_2 production is even less important to subseafloor ecosystems at these sites than indicated by our ratio of radiolytic H_2 production to net respiration at Site 1230.

We infer from these ratios that, in subseafloor sediments, the rate of net respiration is an important indicator of the potential importance of radiolytic H_2 as an electron donor; if net respiration is high, H_2 from radiolysis of water is not a significant electron donor for the ecosystem as a whole. At sites with even lower rates of respiration than the Leg 201 sites, *e.g.*, in a central ocean gyre, H_2 from radiolysis of water may be the principal electron donor for the subseafloor sedimentary ecosystem (D'Hondt *et al.*, 2006; Jørgensen and D'Hondt, 2006).

Similarly, because radiolytic H_2 production in subseafloor sediments does not necessarily change with depth, but net respiration typically decreases with depth as organic matter is depleted, radiolytic H_2 may be an increasingly important source of electron donors with increasing sediment depth and sediment age.

The results of this study provide a basis for predicting the abundance of cells that might occur in a subsurface sedimentary ecosystem where H_2 from water radiolysis is the principal electron donor. At Site 1231, cell abundances averaged 10^6 cells/cm^3 (Shipboard Scientific Party, 2003g). If the number of microbes that rely on radiolytic H_2 is proportional to the fraction of electron donors provided by radiolytic H_2 at Site 1231, our results suggest that $\sim 10^5$ cells/cm^3 ($\sim$9.8% of the Site 1231 total) are fueled by H_2 from water radiolysis. We infer from this calculation that $\sim 10^5$ cells/cm^3 may be supported in a marine sedimentary ecosystem where radiolytic H_2 is the principal electron donor.

A similar approach could be used to predict the abundance of cells that could be sustained by radiolytic hydrogen in wet sedimentary environments on early Earth and other planetary bodies, such as subsurface Mars and sub-ice Europa. In this manner, extant subseafloor ecosystems may be useful models for non-photosynthetic ecosystems on early Earth and for sedimentary ecosystems on other planets.

CONCLUSIONS

Production of H_2 by water radiolysis in subsurface environments depends on concentrations of radioactive elements, porosity, and grain size. In the sediments examined for this study, $\sim$90% of the calculated H_2 production results from alpha decay of uranium and thorium. Comparison of calculated radiolytic H_2 yields to net respiration at multiple sites suggests that radiolysis gains importance as an electron donor source as net respiration and organic carbon content decrease. Production of H_2 by water radiolysis may fuel 10% of the metabolic respiration at the Leg 201 site where organic-fueled respiration is lowest (ODP Site 1231). In sedimentary ecosystems with even lower rates of net respiration, such as in a central ocean gyre, water radiolysis may be the principal source of electron donors. This process has the potential to sustain a subsurface

ecosystem in wet sediments of other planetary bodies, such as Mars and Europa.

ACKNOWLEDGMENTS

We thank Katherine Kelley for advice on the ICP mass spectrometry analyses, Kelly Hanks for assisting with an early version of the radiolytic model, and Tori Hoehler for inviting us to participate in the "Follow the Energy" symposium that led to this special edition of *Astrobiology*.

ABBREVIATIONS

HNGS, Hostile Environment Natural Gamma Ray Sonde; ICP-MS, inductively coupled plasma mass spectrometry; mbsf, meters below seafloor; NGR, natural gamma radiation; ODP, Ocean Drilling Program; QA/QC, quality assurance/quality control; SRM, standard reference material.

REFERENCES

Aitken, M.J. (1985) *Thermoluminescence Dating*, Academic Press, Orlando, FL.

Bacon, M.P. (1984) Glacial to interglacial changes in carbonate and clay sedimentation in the Atlantic Ocean estimated from ^{230}Th measurements. *Isot. Geosci.* 2, 97–111.

Balzer, V. (1999) Late Miocene history of sediment subduction and recycling as recorded in the Nicaraguan volcanic arc. MS thesis, University of Kansas, Lawrence, Kansas.

Boston, P.M., Ivanov, M.V., and McKay, C.P. (1992) On the possibility of chemosynthetic ecosystems in subsurface habitats on Mars. *Icarus* 95, 300–308.

Chapelle, F.H., O'Neill, K., Bradley, P.M., Methe, B.A., Ciufo, S.A., Knobel, L.L., and Lovley, D.R. (2002) A hydrogen-based subsurface microbial community dominated by methanogens. *Nature* 415, 312–314.

Cheatham, M.M., Sangrey, W.F., and White, W.M. (1993) Sources of error in external calibration ICP-MS analysis of geological samples and an improved non-linear drift correction procedure. *Spectrochim. Acta B* 48, E487–E506.

D'Hondt, S., Jørgensen, B.B., Miller, D.J., *et al.* (2003) Controls on microbial communities in deeply buried sediments, eastern equatorial Pacific and Peru Margin Sites 1225–1231. In *Proceedings of the Ocean Drilling Program, Initial Reports,* Vol. 201 [CD-ROM]. Available from Ocean Drilling Program, Texas A & M University, College Station, TX, 77845-9547, USA, doi:10.2973/odp.proc.ir.201.2003.

D'Hondt, S. *et al*. (2004) Distributions of microbial activities in deep subseafloor sediments. *Science* 306, 2216–2221.

D'Hondt, S., Abrams, L.J., Pockalny, R.A., Spivack, A.J., and Teske, A.P. (2006) Subseafloor exploration in the central South Pacific, NASA Astrobiology Institute biennial meeting 2005. *Astrobiology* 6, 201.

Draganic, I.G. and Draganic Z.D. (1971) *The Radiation Chemistry of Water*, Academic Press, New York.

Ekström, L.P. and Firestone R.B. (1999) *World Wide Web Table of Radioactive Isotopes,* database version 2/28/99, from http://ie.lbl.gov/toi/index.htm (last accessed 9/19/2006).

Fisk, M.R. and Giovannoni, S.J. (1999) Sources of nutrients and energy for a deep biosphere on Mars. *J. Geophys. Res.* 105, 11805–11815.

Harris, R.E. and S.M. Pimblott. (2002) On ^{3}H β-Particle and ^{60}Co γ irradiation of aqueous systems. *Radiat. Res.* 158, 493–504.

Hogg, R.V. and Ledolter, J. (1992) *Applied Statistics for Engineers and Physical Scientists*, Macmillan, New York.

Jahnke, RA. (1996) The global ocean flux of particulate organic carbon: areal distribution and magnitude. *Global Biogeochem. Cycles* 10, 71–88.

Jørgensen, B.B. and D'Hondt, S. (2006) A starving majority deep beneath the seafloor. *Science* 314, 932–934.

Kelley, K.A., Plank, T., Ludden, J., and Staudigel, H. (2003) Composition of altered oceanic crust at ODP Sites 801 and 1149. *Geochemistry, Geophysics, Geosystems* 4, 1–21.

Kelley, D.S., *et al.* (2005) A serpentinite-hosted ecosystem: the Lost City Hydrothermal Field. *Science* 307, 1428–1434.

Lin, L., Slater, G.F., Lollar, B.S., Lacrampe-Couloume, G., and Onstott, T.C. (2005) The yield and isotopic composition of radiolytic H_2, a potential energy source for the deep subsurface biosphere. *Geochim. Cosmochim. Acta* 69, 893–903.

Mével, C. (2003) Serpentinization of abyssal peridotites at mid-ocean ridges. *Comptes Rendus Geoscience* 335, 825–852.

Pedersen, K. (1993) Bacterial processes in nuclear waste disposal. *Microbiology Europe* 1, 18–23.

Pedersen, K. (1997) Microbial life in deep granitic rock. *FEMS Microbiol. Rev.* 20, 399–414.

Shipboard Scientific Party. (2003a) Site 1225. In *Proceedings of the Ocean Drilling Program, Initial Reports,* Vol. 201, S.L. D'Hondt, B.B. Jørgensen, D.J. Miller, *et al*., Ocean Drilling Program, College Station, TX, pp. 1–86, doi:10.2973/odp.proc.ir.201.106.2003.

Shipboard Scientific Party. (2003b) Site 1226. In *Proceedings of the Ocean Drilling Program, Initial Reports,* Vol. 201, S.L. D'Hondt, B.B. Jørgensen, D.J. Miller, *et al*., Ocean Drilling Program, College Station, TX, pp. 1–96, doi:10.2973/odp.proc.ir.201.107.2003.

Shipboard Scientific Party. (2003c) Site 1227. In *Proceedings of the Ocean Drilling Program, Initial Reports,* Vol. 201, S.L. D'Hondt, B.B. Jørgensen, D.J. Miller, *et al*., Ocean Drilling Program, College Station, TX, pp. 1–66, doi:10.2973/odp.proc.ir.201.108.2003.

Shipboard Scientific Party. (2003d) Site 1228. In *Proceedings of the Ocean Drilling Program, Initial Reports,* Vol. 201, S.L. D'Hondt, B.B. Jørgensen, D.J. Miller, *et al.*, Ocean Drilling Program, College Station, TX, pp. 1–72, doi:10.2973/odp.proc.ir.201.109.2003.

Shipboard Scientific Party. (2003e) Site 1229. In *Proceedings of the Ocean Drilling Program, Initial Reports,* Vol. 201, S.L. D'Hondt, B.B. Jørgensen, D.J. Miller, *et al.*, Ocean Drilling Program, College Station, TX, pp. 1–78, doi:10.2973/odp.proc.ir.201.110.2003.

Shipboard Scientific Party. (2003f) Site 1230. In *Proceedings of the Ocean Drilling Program, Initial Reports,* Vol. 201, S.L. D'Hondt, B.B. Jørgensen, D.J. Miller, *et al.*, Ocean Drilling Program, College Station, TX, pp. 1–107, doi:10.2973/odp.proc.ir.201.111.2003.

Shipboard Scientific Party. (2003g) Site 1231. In *Proceedings of the Ocean Drilling Program, Initial Reports,* Vol. 201, S.L. D'Hondt, B.B. Jørgensen, D.J. Miller, *et al.*, Ocean Drilling Program, College Station, TX, pp. 1–64, doi:10.2973/odp.proc.ir.201.112.2003.

Skilbeck, C.G. and Fink, D. (2006) Data report: radiocarbon dating and sedimentation rates for Holocene–upper Pleistocene sediments, eastern equatorial Pacific and Peru continental margin. In *Proceedings of the Ocean Drilling Program, Initial Reports,* Vol. 201, edited by B.B. Jørgensen, S.L. D'Hondt, and D.J. Miller, Ocean Drilling Program, College Station, TX, pp. 1–15, doi:10.2973/odp.proc.sr.201.108.2006.

Spinks, J.W.T. and Woods, R.J. (1990) *An Introduction to Radiation Chemistry,* John Wiley & Sons, New York.

Steurer, J.F. and Underwood, M.B. (2003) Data report: the relation between physical properties and grain-size variations in hemipelagic sediments from Nankai Trough. *Proceedings of the Ocean Drilling Program: Scientific Results,* Vol. 190/196, Ocean Drilling Program, College Station, TX.

Stevens, T.O. and McKinley, J.P. (1995) Lithoautotrophic microbial ecosystem in deep basalt aquifers. *Science* 270, 450–453.

Taylor, S. R. and McLennan, S.M. (1985) *The Continental Crust: Its Composition and Evolution,* Blackwell, Oxford.

Wang, G., Spivack, A.J., and D'Hondt, S. (2006) Identification of respiration pathways in deep subseafloor sediments using a CO_2 mass-balance model, NASA Astrobiology Institute Biennial Meeting 2005. *Astrobiology* 6, 230.

Wedepohl, K.H. (1978) *Handbook of Geochemistry*, Springer-Verlag, Berlin.

Address reprint requests to:
Steven D'Hondt
Graduate School of Oceanography
University of Rhode Island
Narragansett, RI 02882

E-mail: dhondt@gso.uri.edu

APPENDIX 1: DERIVATION OF WATER RADIOLYSIS MODEL

The radiation dose equations assume that within a volume of sediment with dimensions larger than the ranges of the emitted radiations, the rate of energy emission due to radioactive decay is equal to the rate of energy absorption by water and sediment particles because energy is conserved (Aitken, 1985).

The energy emitted during decay can be written as

$$F_{e,i} = (\overline{A}_x \Sigma E_{i,x})(1 - \phi)\rho_r$$

$$F_{e,i}[=]\left(\frac{decays}{time * mass_{rock}} * \frac{energy}{decay}\right) * \left(\frac{V_{rock}}{V_{sed}}\right) * \frac{mass_{rock}}{V_{rock}} = \frac{energy}{time * V_{sed}} \quad \text{(A1.1)}$$

where i denotes alpha, beta, or gamma radiation, x denotes a radioactive isotope (e.g. ^{238}U), A_x is the activity of parent nuclide x, $\Sigma E_{i,x}$ is the alpha, beta, or gamma energy sum of the decay series of parent nuclide x (assuming secular equilibrium), ϕ is porosity, and ρ_r is grain density.

The energy absorbed during decay can be written as

$$F_{a,i} = D_{w,i}\phi + D_{r,i}(1 - \phi)$$

$$F_{a,i}[=]\left(\frac{energy}{time * V_{water}} * \frac{V_{water}}{V_{sed}}\right) + \left(\frac{energy}{time * V_{rock}} * \frac{V_{rock}}{V_{sed}}\right) = \frac{energy}{time * V_{sed}} \quad \text{(A1.2)}$$

where $D_{w,i}$ is the radiation dose absorbed by the water and $D_{r,i}$ is the radiation dose absorbed by the sediment grains. Setting Equations A1.1 and A1.2 equal to one another,

$$(\overline{A}_x \Sigma E_{i,x})(1 - \phi)\rho_r = D_{w,i}\phi + D_{r,i}(1 - \phi)$$

We define the relative stopping power ratio, S_i, as $S_i = \frac{D_{w,i}}{D_{r,i}}$. This ratio compares the ability of water to stop a given type of radiation i over the ability of quartz (which is taken to represent the solid phase) to stop the same type of radiation. Substituting this into the above equation,

$$(\overline{A}_x \Sigma E_{i,x})(1 - \phi)\rho_r = D_{w,i}\left(\phi + \frac{D_{r,i}}{D_{w,i}}(1 - \phi)\right) = D_{w,i}\left(\phi + \frac{1}{S_i}(1 - \phi)\right) \quad \text{(A1.3)}$$

Solving for the dose absorbed by the water and simplifying,

$$D_{w,i} = \frac{(\overline{A}_x \Sigma E_{i,x})(1 - \phi)\rho_r}{\phi + \frac{1}{S_i}(1 - \phi)} \quad \text{(A1.4)}$$

$$D_{w,i} = \frac{(\overline{A}_x \Sigma E_{i,x})(1 - \phi)\rho_r}{\phi + \frac{1}{S_i}(1 - \phi)} * \frac{1/(1 - \phi)}{1/(1 - \phi)} = \frac{(\overline{A}_x \Sigma E_{i,x})\rho_r}{\frac{\phi}{(1 - \phi)} + \frac{1}{S_i}} \quad \text{(A1.5)}$$

To convert to the dose absorbed by the bulk sediment, multiply Equation A1.5 by porosity,

$$D_{i,x} = \frac{(\overline{A}_x \Sigma E_{i,x})\rho_r}{\frac{\phi}{(1 - \phi)} + \frac{1}{S_i}} * \phi = \frac{(\overline{A}_x \Sigma E_{i,x})\rho_r}{\frac{1}{(1 - \phi)} + \frac{1}{S_i\phi}} \quad \text{(A1.6)}$$

To summarize the variables,

i. F_e (MeV/s/cm^3) is the energy emitted during radioactive decay.
ii. F_a (MeV/s/cm^3) is the energy absorbed during radioactive decay.
iii. ρ_r (g/cm$^3_{rock}$) is the grain density.
iv. A_x (decays/s/g$_{rock}$) is the activity of parent nuclide *x.*
v. $\Sigma E_{i,x}$ (MeV / decay series) is the alpha, beta, or gamma energy sum of the decay series of parent nuclide *x.*
vi. ϕ is the porosity (volume of water / volume of sediment).
vii. D_w (MeV/s/cm$^3_{H_2O}$) is the radiation dose absorbed by the water.
viii. D_r (MeV/s/cm$^3_{rock}$) is the radiation dose absorbed by the sediment grains.
ix. S_i is the relative stopping power ratio for alpha, beta, or gamma radiation.
x. $D_{i,x}$ (MeV/s/cm$^3_{sed}$) is the radiation dose absorbed by the bulk sediment due to the alpha, beta, or gamma decay of the parent nuclide *x* series.

The following assumptions are made when using the above equations:

i. Within a volume of sediment with dimensions larger than the ranges of the emitted radiations, the rate of energy emission due to radioactive decay is equal to the rate of energy absorption by water and sediment particles because energy is conserved (Aitken, 1985).
ii. Porosity is homogeneous.
iii. Grains are small enough for all alpha and beta particles and gamma radiation to escape without significant energy loss.
iv. Radioactive decay is in secular equilibrium.

APPENDIX 2: RADIOLYTIC H_2 YIELD CALCULATIONS

Equations

Hydrogen production by water radiolysis is due to alpha, beta, and gamma radiation, and can be written as

$$P_{H_2sed} = P_{H_2,\alpha} + P_{H_2,\beta} + P_{H_2,\gamma} = (G_{H_2,\alpha}D_\alpha) + (G_{H_2,\beta}D_\beta) + (G_{H_2,\gamma}D_\gamma) \quad \text{(A2.1)}$$

where $G_{H_2,\alpha}$, $G_{H_2,\beta}$, and $G_{H_2,\gamma}$ are the radiation chemical yields of H_2 produced in pure water by radiolysis and D_α, D_β, D_γ are the radiation doses absorbed by the bulk sediment due to alpha, beta, and gamma radiation, respectively.

The radiation dose for a given type of radiation is due to contributions from the decay series of ^{238}U, ^{235}U, ^{232}Th, and ^{40}K:

$$D_\alpha = D_{\alpha,^{238}U} + D_{\alpha,^{235}U} + D_{\alpha,^{232}Th} \quad \text{(A2.2a)}$$

$$D_\beta = D_{\beta,^{238}U} + D_{\beta,^{235}U} + D_{\beta,^{232}Th} + D_{\beta,^{40}K} \quad \text{(A2.2b)}$$

$$D_\gamma = D_{\gamma,^{238}U} + D_{\gamma,^{235}U} + D_{\gamma,^{232}Th} + D_{\gamma,^{40}K} \quad \text{(A2.2c)}$$

Note that the alpha radiation dose does not include a contribution from ^{40}K because this isotope does not undergo alpha decay. Using Equations A2.2a–2c, Equation A2.1 can be rewritten as

$$P_{H_2sed} = [G_{H_2,\alpha}(D_{\alpha,^{238}U} + D_{\alpha,^{235}U} + D_{\alpha,^{232}Th})] + [G_{H_2,\beta}(D_{\beta,^{238}U} + D_{\beta,^{235}U} + D_{\beta,^{232}Th} + D_{\beta,^{40}K})] + [G_{H_2,\gamma}(D_{\gamma,^{238}U} + D_{\gamma,^{235}U} + D_{\gamma,^{232}Th} + D_{\gamma,^{40}K})] \quad \text{(A2.3)}$$

The radiation doses can be expressed using measurable quantities:

$$D_{i,^{238}\mathrm{U}} = \frac{\rho_r \overline{A}_{^{238}\mathrm{U}} \Sigma E_{i^{238}\mathrm{U}}}{\frac{1}{1-\phi} + \frac{1}{S_i \phi}} \quad \text{(A2.4a)}$$

$$D_{i,^{235}\mathrm{U}} = \frac{\rho_r \overline{A}_{^{235}\mathrm{U}} \Sigma E_{i^{235}\mathrm{U}}}{\frac{1}{1-\phi} + \frac{1}{S_i \phi}} \quad \text{(A2.4b)}$$

$$D_{i,^{232}\mathrm{U}} = \frac{\rho_r \overline{A}_{^{232}\mathrm{U}} \Sigma E_{i^{232}\mathrm{U}}}{\frac{1}{1-\phi} + \frac{1}{S_i \phi}} \quad \text{(A2.4c)}$$

$$D_{i,^{40}\mathrm{U}} = \frac{\rho_r \overline{A}_{^{40}\mathrm{U}} \Sigma E_{i^{40}\mathrm{U}}}{\frac{1}{1-\phi} + \frac{1}{S_i \phi}} \quad \text{(A2.4d)}$$

Simplifying,

$$D_\alpha = \frac{\rho_r}{\frac{1}{1-\phi} + \frac{1}{S_\alpha \phi}} \left(\overline{A}_{^{238}\mathrm{U}} \Sigma E_{\alpha,^{238}\mathrm{U}} + \overline{A}_{^{235}\mathrm{U}} \Sigma E_{\alpha,^{235}\mathrm{U}} + \overline{A}_{^{232}\mathrm{Th}} \Sigma E_{\alpha,^{232}\mathrm{Th}}\right) \quad \text{(A2.5a)}$$

$$D_\beta = \frac{\rho_r}{\frac{1}{1-\phi} + \frac{1}{S_\beta \phi}} \left(\overline{A}_{^{238}\mathrm{U}} \Sigma E_{\beta,^{238}\mathrm{U}} + \overline{A}_{^{235}\mathrm{U}} \Sigma E_{\beta,^{235}\mathrm{U}} + \overline{A}_{^{232}\mathrm{Th}} \Sigma E_{\beta,^{232}\mathrm{Th}} + \overline{A}_{^{40}\mathrm{K}} \Sigma E_{\beta,^{40}\mathrm{K}}\right) \quad \text{(A2.5b)}$$

$$D_\gamma = \frac{\rho_r}{\frac{1}{1-\phi} + \frac{1}{S_\gamma \phi}} \left(\overline{A}_{^{238}\mathrm{U}} \Sigma E_{\gamma,^{238}\mathrm{U}} + \overline{A}_{^{235}\mathrm{U}} \Sigma E_{\gamma,^{235}\mathrm{U}} + \overline{A}_{^{232}\mathrm{Th}} \Sigma E_{\gamma,^{232}\mathrm{Th}}\right) + \overline{A}_{^{40}\mathrm{K}} \Sigma E_{\gamma,^{40}\mathrm{K}}\right) \quad \text{(A2.5c)}$$

Variables

P_{H_2sed} (molecules/s/cm$^3_{sed}$) is the production rate of hydrogen.
$G_{H_2,\alpha} = 1.57 \times 10^4$ H_2 molecules/MeV and is the radiation chemical yield for alpha particles (Spinks and Woods, 1990).
$G_{H_2,\beta} = 5.3 \times 10^3$ H_2 molecules/MeV and is the radiation chemical yield for beta particles (Spinks and Woods, 1990).
$G_{H_2,\gamma} = 4.5 \times 10^3$ H_2 molecules/MeV and is the radiation chemical yield for gamma radiation (Spinks and Woods, 1990).
D_α, D_β, D_γ (MeV/s/cm$^3_{sed}$) are the radiation doses absorbed by the bulk sediment due to alpha, beta, and gamma radiation, respectively.
ρ_r (g/cm^3) is the grain density.
$A_{^{238}\mathrm{U}}$, $A_{^{235}\mathrm{U}}$, $A_{^{232}\mathrm{Th}}$, and $A_{^{40}\mathrm{K}}$ (decays/s/g$_{rock}$) are the activities of ^{238}U, ^{235}U, ^{232}Th, and ^{40}K, respectively.
ΣE_α, ΣE_β, ΣE_γ (MeV / decay series) are the alpha, beta, and gamma decay energy sums, respectively, of the decay series of the parent nuclide specified.
ϕ is the porosity (volume of water / volume of sediment).
S_α, S_β, S_γ are the relative stopping power ratios for alpha and beta particles and gamma radiation (a ratio of the ability of water to stop a given type of radiation over the ability of quartz to stop the same type of radiation).

Steps to complete these calculations

1. Obtain necessary data
   a. ^{238}U, ^{235}U, ^{232}Th, and ^{40}K concentrations
      i. use isotopic abundance values to convert ^{39}K or total K abundance to ^{40}K abundance (if needed)
         1. $X_{^{40}\mathrm{K}} = 1.17 \times 10^{-4}$ (from Wedepohl, 1978)

ii. use isotopic abundance values to convert ^{238}U or total U abundance to ^{235}U abundance (if needed)
1. $X_{238U} = 0.99275$, $X_{235U} = 0.00725$ (from Wedepohl, 1978)
iii. $X_{232Th} = 1.00$ (from Wedepohl, 1978)
b. Porosity
c. Grain density
2. Calculate dose rates
a. Convert concentrations to activities using Avogadro's number and each isotope's decay constant
b. Calculate decay energy sums (ΣE_α, ΣE_β, ΣE_γ); in this study they were calculated using the World Wide Web Table of Radioactive Isotopes (Ekström and Firestone, 1999):

	Alpha decay energy sum (MeV/decay)	*Beta decay energy sum (MeV/decay)*	*Gamma decay energy sum (MeV/decay)*
^{40}K	0	1.1760	0.1566
^{232}Th	35.95	2.8408	2.2447
^{238}U	42.87	6.0935	1.7034
^{235}U	34.03	10.4470	0.5500

c. S_i values of 1.5, 1.25, and 1.14 were used for alpha, beta, and gamma radiation, respectively, and were taken from Aitken (1985)
3. Calculate radiolytic H_2 production rates
a. G_{H2} values are from Spinks and Woods (1990), and were converted from μmol/J to H_2 molecules/MeV:

$G_{H_2,\alpha}$	0.163	μmol/J	15719.7852	#H_2 molecules/MeV
$G_{H_2,\gamma}$	0.047	μmol/J	4532.6988	#H_2 molecules/MeV
$G_{H_2,\beta}$	0.055	μmol/J	5304.222	#H_2 molecules/MeV

b. multiply each dose rate by the appropriate G value